Available online at www.sciencedirect.com
SCIENCE DIRECT®
Journal of Power Sources 117 (2003) 203–211
JOURNAL OF POWER SOURCES
www.elsevier.com/locate/jpowsour

Thick-film nickel–metal-hydride battery based on porous ceramic substrates

Jing-Shan Do*, Sen-Hao Yu, Suh-Fen Cheng

Department of Chemical Engineering, Tunghai University, Taichung 40704, Taiwan, ROC

Received 16 October 2002; accepted 17 December 2002

Abstract

Nickel–metal-hydride (Ni–MH) batteries are prepared with thick-film and thin-film technologies based on porous ceramic substrates. The porosity and the mean pore diameter of BP ceramic substrates prepared from the argils increases from 19.81% and 0.0432 μm to 29.81% and 0.224 μm, respectively, upon increasing the ethyl cellulose content in the BP argil from 0 to 0.79%. The pore diameter of Al_2O_3 substrates prepared from Al_2O_3 powder is mainly distributed in the range 0.01–0.5 μm. The distribution of the pore diameters of BP ceramic substrates lies in two ranges, namely: 0.04–2 μm and 10–300 μm. Using BP ceramic plates and Al_2O_3 plates as substrates to fabricate thick-film Ni–MH batteries, the optimal electroactive material utilization in the batteries is 77.0 and 71.1%, respectively. On increasing the screen-printing number for preparing the cathode ($Ni(OH)_2$) from 1 to 3, the discharge capacity of the thick-film battery increases from 0.2917 to 0.7875 mAh, and the utilization in the battery decreases from 71.0 to 53.0%.

Keywords: Nickel–metal-hydride; Thick-film battery; Ceramic substrate; Charge–discharge properties; Porosity; Mean pore diameter

1. Introduction

The power requirements of electronic devices have been reduced due to advances made by the microelectronics industry. The reduction in size and power requirement of various electronic devices, such as personal digital assistant (PDA) units, wireless telecommunications devices and the other microdevices, is the main driving force for developing microbatteries.

The advantages of using microfabrication technologies to prepare batteries are: (i) standardization of the preparation procedures enables easy control of battery quality compared with conventional procedures; (ii) procedures for fabricating batteries can be compatible with those for producing microelectronic devices. There are many reports of lithium and lithium-ion microbatteries that are prepared with thin-film technology [1–13]. These cells are generally a few micrometers thick. The low charge capacity due to the small amount of active material per area requires the cells to have large footprints to provide the power and energy demanded by many applications [14]. Microscopic nickel–zinc batteries are prepared using thick-film technologies [14]. A thicker porous electrode and a liquid electrolyte are used to maximize the power and energy per area. The footprint and the capacity of such microbatteries are 0.02 cm^2 and about 0.555 mWh cm^{-2}, respectively.

In 1990, a nickel–metal-hydride (Ni–MH) battery was commercialized in Japan [15]. Currently, Ni–MH batteries and the Li-ion batteries are used widely in information and communications equipment. The Ni–MH battery has the advantages of very competitive power density and price. Therefore, the Ni–MH rechargeable batteries are promising candidates for autonomous microsystems as micropower supplies. Nevertheless systematic preparation and characterization of the Ni–MH battery by using microfabrication technologies has been seldom reported.

Microfabrication technologies are used to produce thick-film Ni–MH batteries based on porous substrates prepared by an annealing process. Thin-film and thick-film technologies are used to prepare current-collectors, as well as porous electrodes which contain active materials on porous ceramic substrates. In this study, porous substrates are prepared and the utilization of thick-film Ni–MH batteries based on these substrates is characterized and discussed.

* Corresponding author. Tel.: +886-6-2359-0262; fax: +886-6-2350-0255.
E-mail address: jsdo@mail.thu.edu.tw (J.-S. Do).

0378-7753/03/$ – see front matter © 2003 Published by Elsevier Science B.V.
doi:10.1016/S0378-7753(03)00014-4

2. Experimental

2.1. Preparation of ceramic substrates

Porous ceramic plates used as substrates for preparing test cells were obtained commercially (HE2424B and HE2424C, LEATEC Fine Ceramics) and prepared from the argils and the alumina powder, respectively. The porous substrates prepared from the argil (Big Porcelain, AARDVARK) and alumina powder are termed as BP and AL substrates, respectively.

The BP argil was made into the desired geometric plate with a suitable mould and then dried at room temperature and at 70 °C for 2 and 24 h, respectively. Finally, the BP ceramic plates were obtained by means of the annealing procedure shown in Fig. 1a. The final annealing temperature was 1100 °C. The thicknesses of the BP ceramic plates and commercial plates (HE2424B and HE2424C) were 0.75 and 0.635 mm, respectively.

The alumina powder was precipitated from a solution by mixing 0.2 M sodium aluminate and 0.05 M aluminum nitrate aqueous solutions. The Al_2O_3 powder was then filtered, washed with deionized water several times, and dried at room temperature. The desired amount of alumina powder with a particle size less than 200 mesh was screened and placed in a stainless-steel mould with a diameter of 1.3 cm. The alumina plate was then obtained by compacting the powder under a suitable pressure and annealing with the procedure shown in Fig. 1b to obtain the AL series substrate.

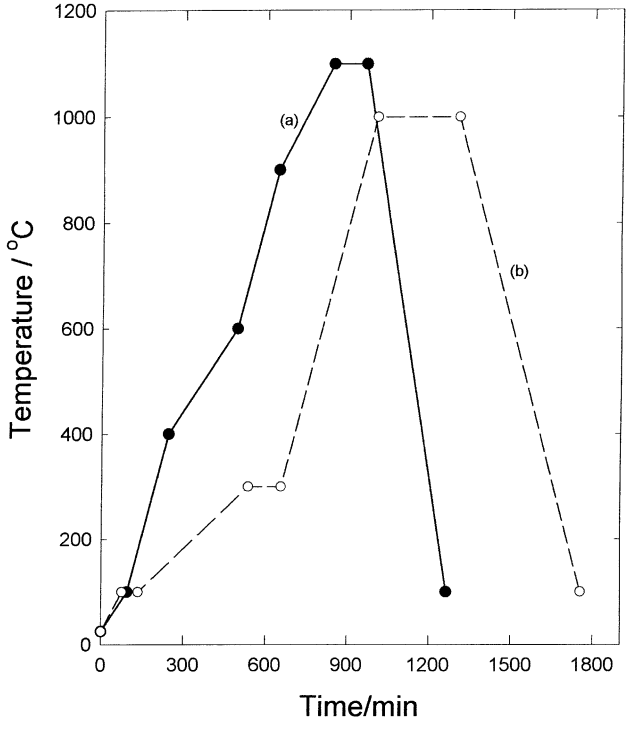

Fig. 1. Relationship of annealing temperature and time: (a) preparation of BP ceramic substrates; (b) preparation of alumina substrates.

The BET surface area and the pore structure of the porous substrates were analyzed by gas adsorption (Micromeritics GEMINI-2375) and mercury intrusion porosimetry (Micromeritics Autopore II 9220), respectively. The surface morphologies of the porous substrates were analyzed with a scanning electron microscope (TOPCON ABT-150S).

2.2. Cell description and fabrication

The cathodic and anodic electrodes of the cell were placed either side of the porous substrate. The latter also played the role of the separator for the conventional battery. The current-collectors were prepared on both sides of porous substrate by sputtering technology and the electroactive materials for the anode and the cathode were then screen-printed on the current-collectors. The paste of the anodic (negative) electrode for screen-printing was obtained by mixing 5 g of metal hydride ($M_mNi_{3.82}Co_{0.52}Mn_{0.50}Al_{0.26}$, CDK-21, Chuo Denki Kogyo) and 0.5 ml of binder solution which was prepared by mixing 1 g of polyvinyl alcohol (PVA, MW 22000, ACROS) with 45 ml of distilled water and stirred at 60 °C until the volume of the solution decreased to 37 ml. The composition of the screen-printing paste for preparing cathodic (positive) electrode were 5 g $Ni(OH)_2$ powder (ACROS), 0.5 g Co powder and 3 ml binder solution. The average diameters of $Ni(OH)_2$ powder, milled in a ball mill (Hsing-Kwang UBM-1) for 120 h, and Co powder were found to be 3.69 and 8.42 μm, respectively.

Electric wires were pasted on the bonding pads of the substrate by a silver paste. The top portions of the two electrodes located at the counter sides of the substrate were covered with epoxy resin, but the edges of the porous substrates were exposed to the electrolyte solution in order to impregnate the electrolyte.

2.3. Cell testing

The charge/discharge capacity of the test cell was measured by a battery cycler (QuickCycler 4.0). The tests were conducted using constant-current charging and discharging. The test cell was charged at the 0.1 C rate to 100% theoretical capacity and discharged at 0.02 C to 0.95 V. Both the anode and cathode had an area of 1.0 cm^2.

3. Results and discussion

3.1. Characterization of porous ceramic substrates

3.1.1. Commercial and BP ceramic plates

The morphologies of BP ceramic plates are shown in Fig. 2. A rough surface morphology was found for the BP plate annealed in the final step at 800 °C (BP800), Fig. 2a. Some fibrous structure was found in the BP ceramic plate on annealing at 900 °C (BP900), Fig. 2b. Increasing the annealing temperature in the final step to 1000 °C (BP1000)

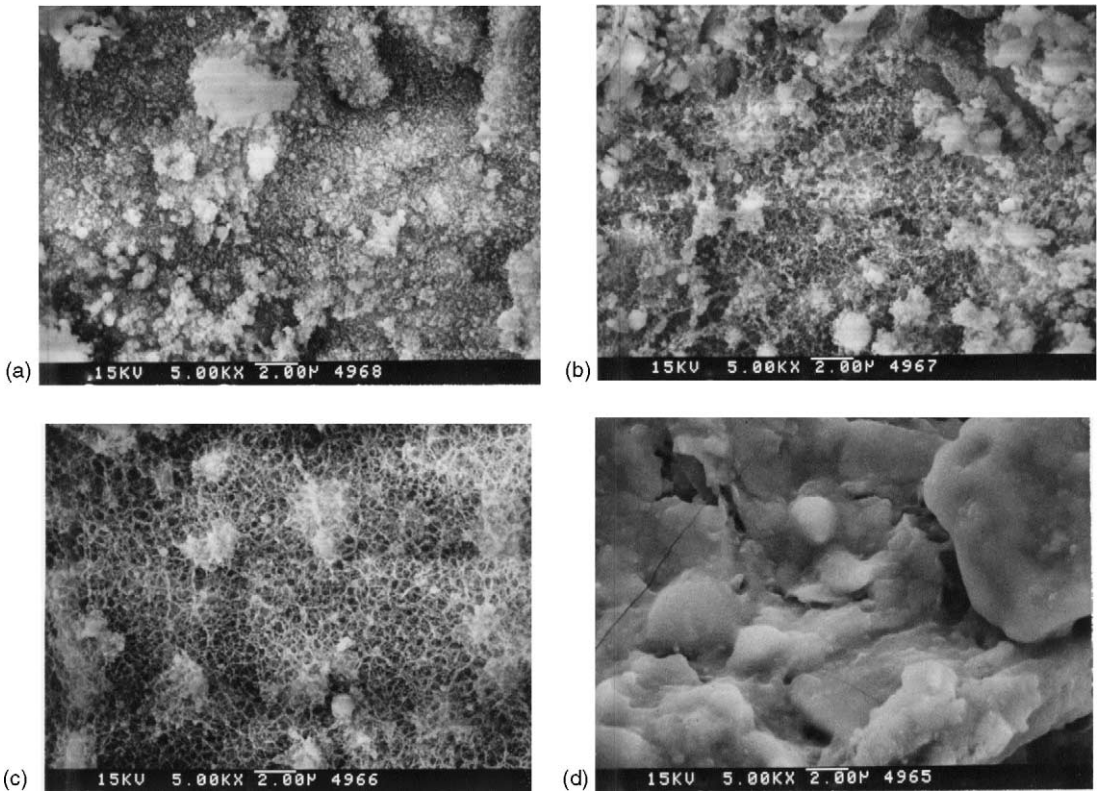

Fig. 2. Electron micrographs of BP ceramic plates. Annealing temperature: (a) 800 °C (BP800); (b) 900 °C (BP900); (c) 1000 °C (BP1000); (d) 1100 °C (BP1100).

increased the fibrous structure on the surface Fig. 2b and c. When the annealing temperature is increased to 1100 °C, melted fragments are found on the substrate, Fig. 2d. These results indicate that a denser substrate is obtained by increasing the annealing temperature. This observation can be demonstrated by BET surface area analysis, as shown in Table 1. Upon increasing the annealing temperature in the final step from 800 to 1000 °C, the surface area decreases from 11.40 to 6.89 $m^2\ g^{-1}$. Further increase of the annealing temperature to 1100 °C decreases the surface area sharply to 0.57 $m^2\ g^{-1}$ (Table 1). It is also found that the mechanical properties of BP ceramic plates decrease upon decreasing the annealing temperature in the final step. When the annealing temperature is less than 1000 °C, the poor mechanical properties caused cracks in the BP ceramic substrates during screen-printing of the electrodes. The BET surface area of the commercial product HE2424B is similar to that of BP1100. The other commercial product

Table 1
BET surface area of BP and commercial ceramic substrates

Substrate	BET surface area ($m^2\ g^{-1}$)
BP800	11.40
BP900	10.22
BP1000	6.89
BP1100	0.57
HE2424B	0.54
HE2424C	1.59

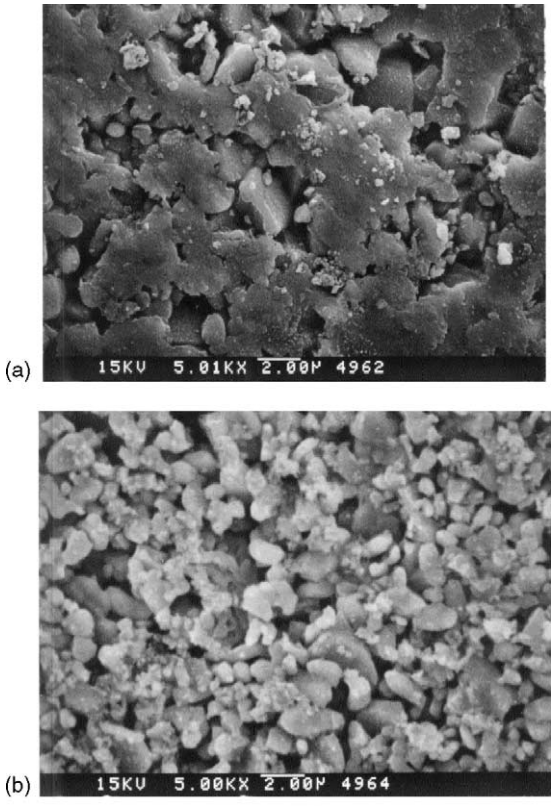

Fig. 3. Electron micrographs of commercial ceramic plates: (a) HE2424B; (b) HE2424C.

HE2424C displays a more porous structure compared with HE2424B and BP1100, as shown in Table 1 and Fig. 3.

3.1.2. Alumina plates

When 0.5 g alumina powder was used to press the alumina plate annealed with procedure shown in Fig. 1b, the surface structure became more compact and denser with increasing the pressure from 2.26×10^7 to 3.77×10^7 kg m^{-2} (Fig. 4a–c). This result could also be demonstrated from the decrease of the thickness of alumina plate with increasing the pressure. The thickness of alumina plate decreased from 2.06 to 1.65 mm when the pressure increased from 2.26×10^7 to 3.77×10^7 kg m^{-2} and the weight of alumina powder was 0.50 g (Fig. 5).

On the other hand, similar surface morphologies of alumina plates (AL53, AL43 and AL33) were observed in electron micrographs (Fig. 4c–e) when the pressure for preparing alumina plate was set at 3.77×10^7 kg m^{-2} and the weight of the alumina powder decreased from 0.5 to 0.3 g. The thickness of alumina plate decreased from 1.65 to 1.02 mm when the weight of alumina powder decreased from 0.5 to 0.3 g at a pressure of 3.77×10^7 kg m^{-2} (Fig. 5). The pore size of alumina plates prepared with 0.5 g alumina powder at a pressure of 2.26×10^7 kg m^{-2} (AL51) was mainly between at 0.01 and 0.5 μm, as shown in Fig. 6. The mean pore diameter of the AL51 alumina plate was 0.0264 μm (Table 2).

3.1.3. Effect of cellulose on characteristics of BP plates

The ethyl cellulose contained in the BP argil will be decomposed and reacted with oxygen during the annealing process. Therefore, the porosity of the BP substrate was

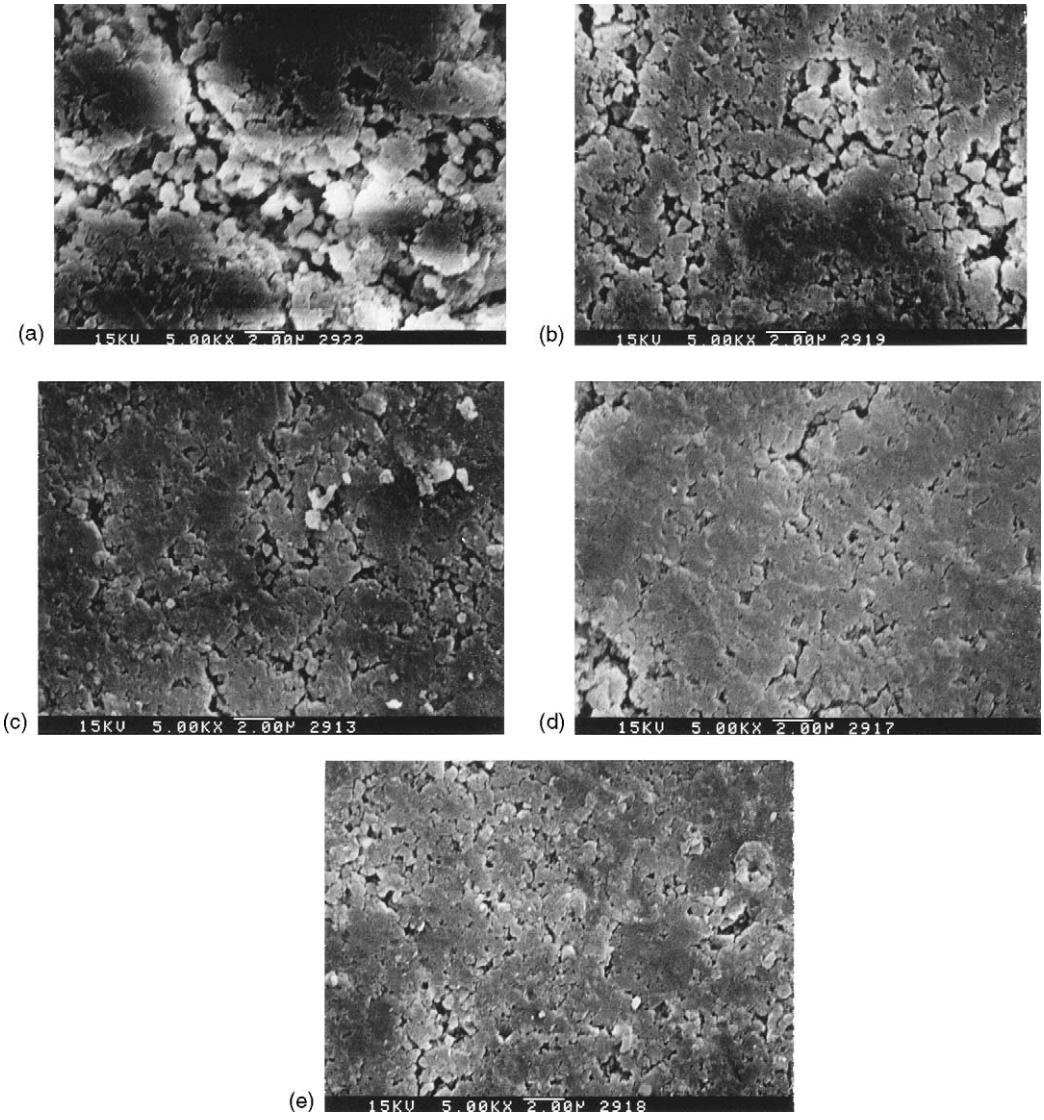

Fig. 4. Electron micrographs of alumina plates: (a) AL51, Al_2O_3, 0.5 g, pressure for pressing, 2.26×10^7 kg m^{-2}; (b) AL52, Al_2O_3, 0.5 g, pressure for pressing, 3.01×10^7 kg m^{-2}; (c)AL53, Al_2O_3, 0.5 g, pressure for pressing, 3.77×10^7 kg m^{-2}; (d) AL43, Al_2O_3, 0.4 g, pressure for pressing, 3.77×10^7 kg m^{-2}; (e) AL33, Al_2O_3, 0.3 g, pressure for pressing, 3.77×10^7 kg m^{-2}.

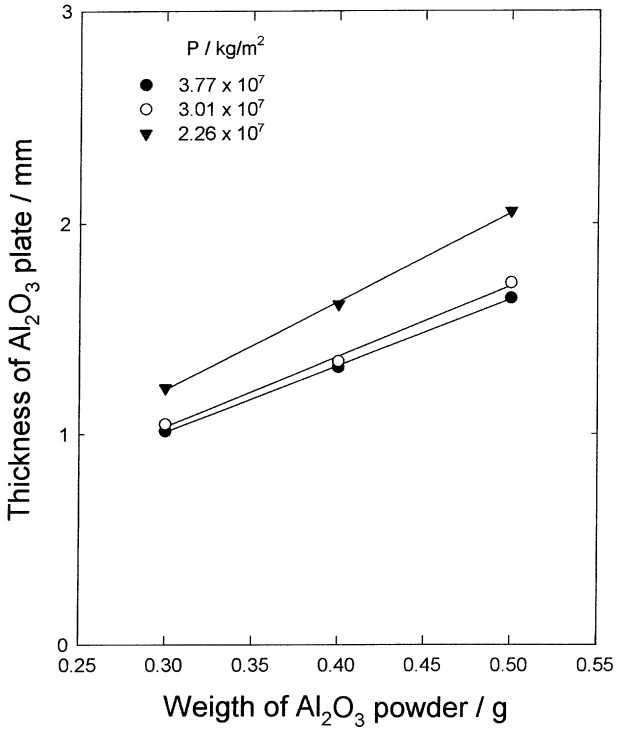

Fig. 5. Effect of weight of Al_2O_3 powder on thickness of Al_2O_3 plate for various pressing pressures.

expected to increase with addition of ethyl cellulose into the argil. BP-C40 and BP-C79 plates were prepared by adding 0.40 and 0.79%, respectively, (based on the dried argil) ethyl cellulose into the BP argil, and were prepared as described in Section 2. The annealing temperature in the final step was controlled at 1100 °C. Compared with BP1100, the surface morphologies of BP-C series plates became rougher and some large pores on the surface of substrate were observed in the electron micrographs, as shown in Fig. 7.

Table 2
Analysis of substrates by means of mercury intrusion porosimetry

Substrate	Pore volume (ml g^{-1})	Mean pore diameter (μm)	Porosity (%)
AL51	0.406	0.0264	56.11
BP1100	0.0922	0.0432	19.81
BP-C40	0.133	0.161	25.82
BP-C79	0.164	0.224	29.81

Two ranges of pore-size distribution of BP ceramic plates were found from the mercury intrusion analysis, as shown in Fig. 8, namely: 0.04–2 μm and 10–300 μm. Increasing the content of ethyl cellulose in the BP argil increases the fraction of pore size in the range of 10–300 μm. The experimental results reveal that the larger pores of substrate are mainly due to the ethyl cellulose in the BP argil. As shown in Table 2, the mean pore diameter increases from 0.0432 to 0.224 μm with increase in the content of ethyl cellulose in the BP argil from 0 to 0.79%. Increasing the content of ethyl cellulose from 0 to 0.79% also causes an increase in the pore volume and in the porosity from 0.0922 ml g^{-1} and 19.81% to 0.164 ml g^{-1} and 29.81% (Table 2). Although the pore volume and porosity of the alumina plate AL51 (0.406 ml g^{-1} and 56.11%) are greater than those of the BP series plates, the mean pore diameter of AL51 (0.0264 μm) is less than that of BP series substrates because the pore size of AL51 substrate is mainly distributed in the range 0.01–0.5 μm.

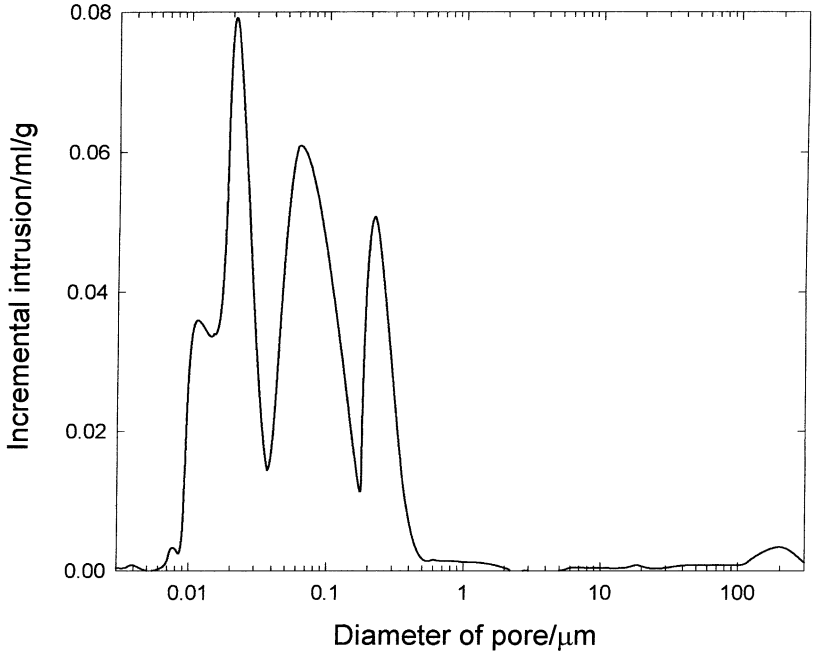

Fig. 6. Mercury intrusion analysis of Al_2O_3 plate (AL51).

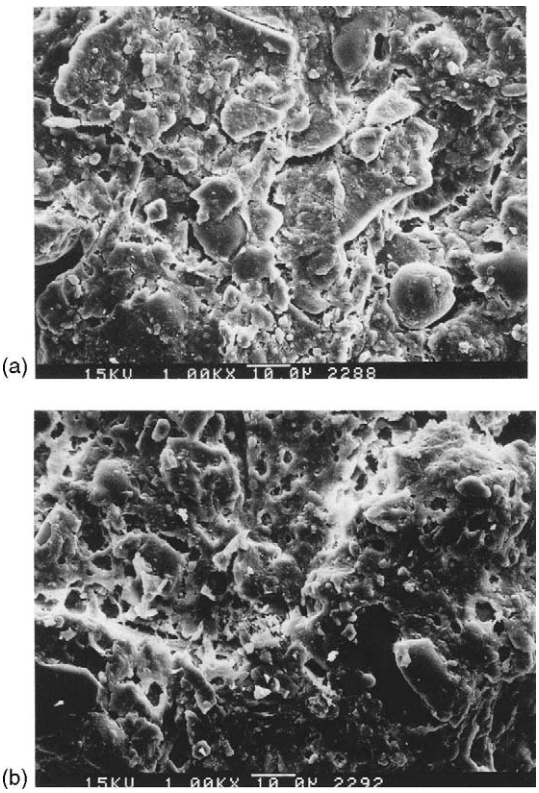

Fig. 7. Electron micrographs of BP-C40 and BP-C79 plates: (a) BP-C40; (b) BP-C79.

3.2. Charge–discharge properties of batteries

The amount of electroactive material, $Ni(OH)_2$, printed on the cathodic (positive) electrode is less than that of metal hydride printed on the anodic (negative) electrode. Therefore, the cathode is the limiting electrode of the battery and the theoretical discharge capacity of the battery is calculated based on the weight of $Ni(OH)_2$ printed on the cathode. The electroactive material utilization in the battery is evaluated according to the following equation:

$$\text{utilization}\,(\%) = \frac{\text{discharge capacity}}{\text{theoretical discharge capacity}} \times 100 \quad (1)$$

3.2.1. Effect of time for impregnation of electrolyte

The battery prepared as described in Section 2 was placed in 5.34 M KOH and 0.477 M LiOH aqueous solution to impregnate the electrolyte at a reduced pressure of 0.033 atm. Using HE2424C as the substrate, the discharge capacity and the utilization in the battery increases from 1.002 mAh and 18.06% to 1.618 mAh and 29.16% with increase in the charge–discharge cycle number from 1 to 3 when the electrolyte impregnation time is fixed at 12 h (Fig. 9). On the fourth cycle, the discharge capacity and the utilization of the battery does not change significantly. The experimental results indicate that the formation reaction of the battery stabilizes the properties of battery over the first three cycles. On increasing the impregnation time to 24 h, the relationship between the utilization of the battery and the cycle number is similar to that obtained for an impregnation time of 12 h. This observation indicates that the adsorption of electrolyte into the battery reaches a saturation level and the effect of impregnation time on the utilization of the battery is insignificant when the impregnation time is greater than 12 h.

When HE2424B is used as a substrate to fabricate the battery, the discharge capacity and the utilization of

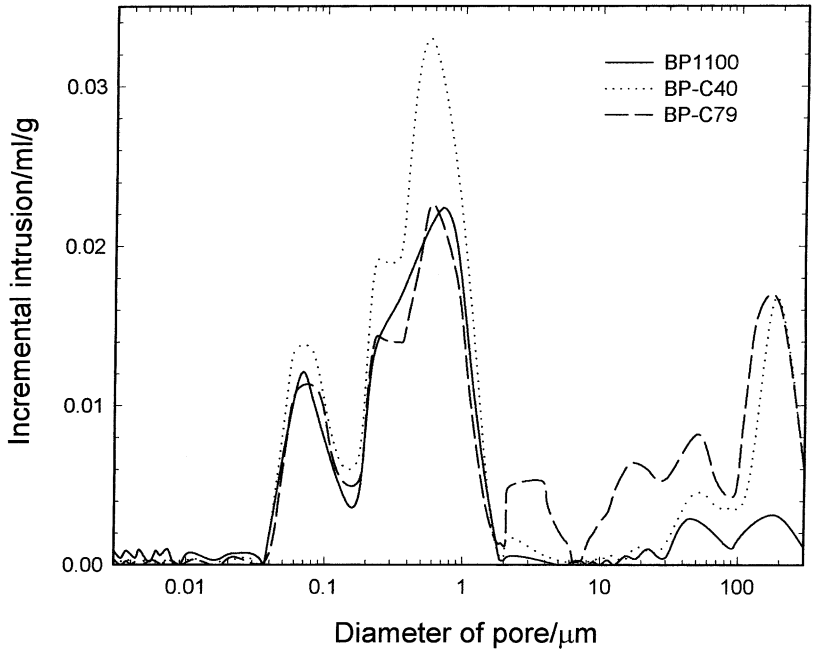

Fig. 8. Mercury intrusion analysis of BP ceramic plates.

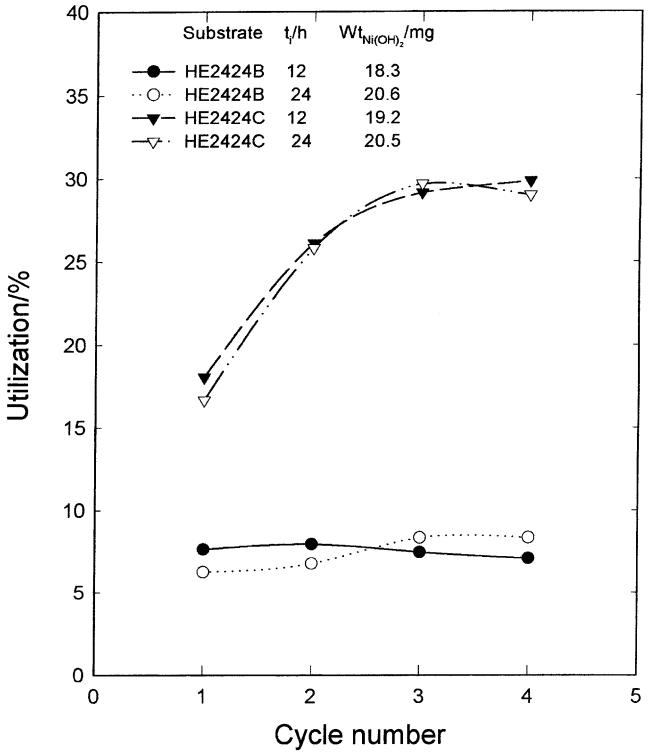

Fig. 9. Effect of cycle number on electroactive material utilization for various impregnating time and substrates. Charge conditions: 0.05 C charged to 100% SoC. Discharge conditions: 0.025 C discharged to 0.95 V. Electrolyte: 5.347 M KOH and 0.477 M LiOH aqueous solution.

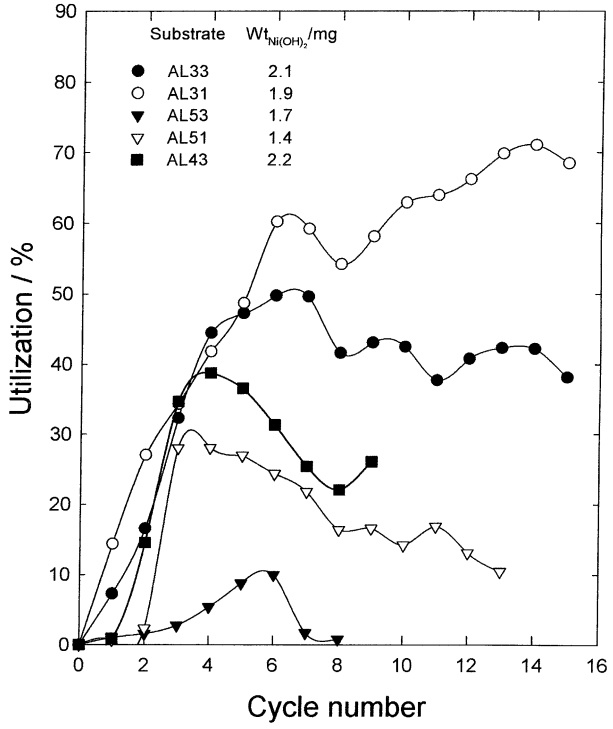

Fig. 10. Effect of cycle number on electroactive material utilization in batteries based on alumina substrates. Charge conditions: 0.10 C charged to 100% SoC. Discharge conditions: 0.02 C discharged to 0.95 V. Electrolyte: 5.347 M KOH and 0.477 M LiOH aqueous solution.

battery are both much less than when using HE2424C as a substrate. Compared with HE2424B, the more porous structure of HE2424C causes greater BET surface area and porosity. Therefore, the electrolyte content of the battery based on HE2424C is greater than that in a battery based on HE2424B. Accordingly, the internal resistance and the electroactive material utilization in the battery based on HE2424C are greater than those for the battery based on HE2424B.

3.2.2. Batteries based on Al_2O_3 substrate

The porosity of the alumina substrate decreases with increase in the pressure used for preparing alumina plates (AL51, AL52 and AL53), as shown in the electron micrographs presented in Fig. 4a–c. The ionic transfer rate decreases and the internal resistance of the battery increases with decrease in the porosity of the alumina plates. Using the same pressure with various amounts of alumina powder to prepare the alumina plates, similar surface morphologies and porosity of the alumina substrates (AL53, AL43 and AL33) are obtained as illustrated in Fig. 4c–e. The thickness of the alumina substrate increases with increase in the amount of alumina powder used for preparing plates at the same pressure, as shown in Fig. 5. The increase in the thickness of the substrate causes an increase in the internal resistance of the battery. The cycle number for obtaining maximum electroactive material utilization in batteries based on various alumina substrates is also different, as demonstrated in Fig. 10. The maximum utilization in a battery based on the alumina substrate decreases from 71.1 to 49.8% with increase in the pressure used for preparation of the alumina substrate from 2.26×10^7 to 3.77×10^7 kg m^{-2} when the weight of the alumina powder is 0.3 g. Increasing the weight of alumina powder from 0.3 to 0.5 g decreases the maximum utilization in battery from 49.8 to 10.0% when the pressure for preparing substrate is set at 3.77×10^7 kg m^{-2} (Fig. 10).

3.2.3. Batteries based on BP ceramic substrates

When the annealing temperature for preparing BP ceramic substrates is less than 1000 °C, the mechanical properties of the substrate become unsatisfactory for the fabrication of batteries. Therefore, BP argils containing various amounts of ethyl cellulose have been annealed at 1100 °C and used as substrates in batteries. Increasing the amount of ethyl cellulose in the BP argils from 0 to 0.79%, the pore volume, the mean pore diameter and the porosity of the BP ceramic substrates increase from 0.0922 ml g^{-1}, 0.0432 μm and 19.81% to 0.164 ml g^{-1}, 0.224 μm and 29.61%, respectively, as illustrated in Table 2. The internal resistance of batteries based on the BP ceramic substrates is therefore expected to decrease with increase in the content of ethyl cellulose in the BP argils. The cycle number for the batteries to reach steady discharge capacities is found to

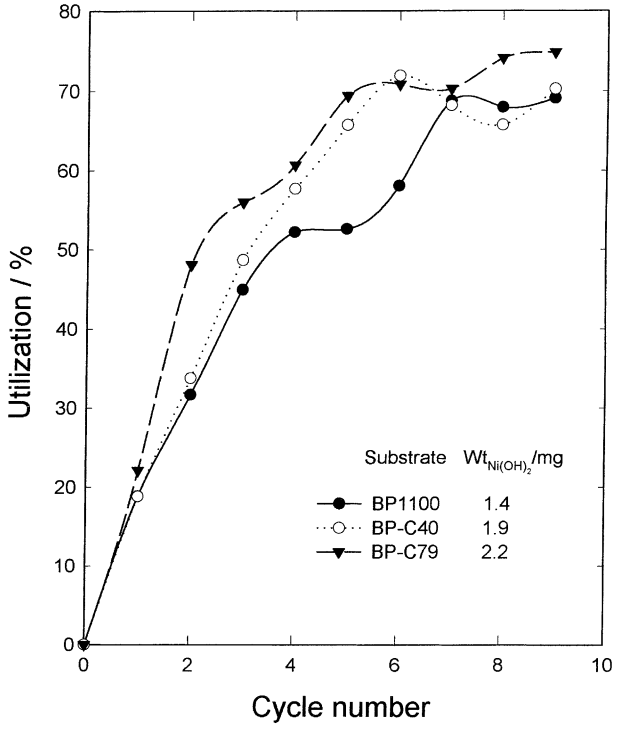

Fig. 11. Effect of cycle number on electroactive material utilization in batteries based on BP ceramic substrates. Charge conditions: 0.10 C charged to 100% SoC. Discharge conditions: 0.02 C discharged to 0.95 V. Electrolyte: 5.347 M KOH and 0.477 M LiOH aqueous solution. Time for impregnation of electrolyte: 12 h.

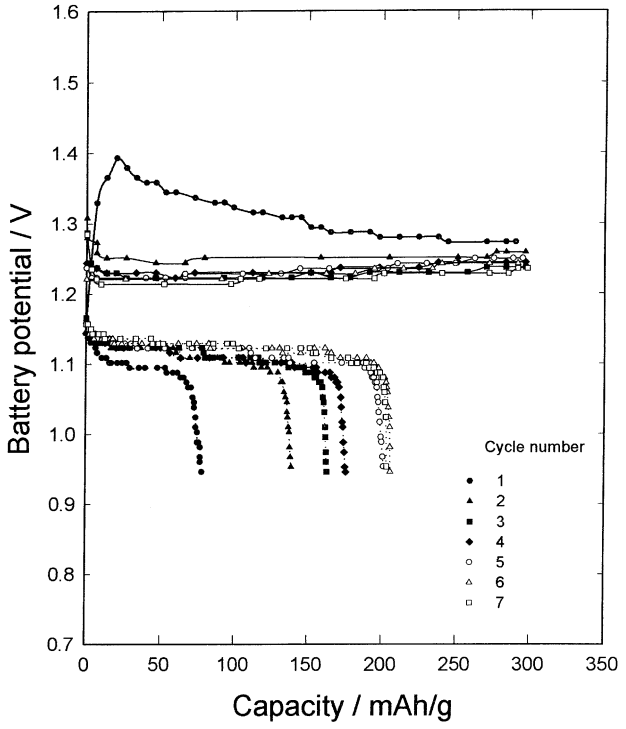

Fig. 12. Charge–discharge curves for various cycle numbers. Charge conditions: 0.10 C charged to 100% SoC. Discharge conditions: 0.02 C discharged to 0.95 V. Electrolyte: 5.347 M KOH and 0.477 M LiOH aqueous solution. Substrate: BP-C79. Weight $Ni(OH)_2$: 2.2 mg. Time for impregnation of electrolyte: 12 h.

decrease from 7 to 5, and the maximum utilization of batteries increases from 68.8 to 74.9% with the increase in the amount of ethyl cellulose in the BP argil from 0 to 0.79% (Fig. 11). The decrease in the formation cycle number and the increase in the discharge capacity are due to a decrease in the internal resistance of the batteries when the content of ethyl cellulose in the BP argils is increased.

The voltage for charging a battery with the BP-C79 substrate decreases with cycle number, as shown in Fig. 12. On the other hand, the discharge voltage increases with cycle number. Finally, the charge and discharge voltages of the battery approach stable values. The experimental results indicate that the internal resistance of the battery decreases with cycle number and the characteristics of the battery finally approach those for stable conditions. A discharge potential plateau is found in the range 1.13–1.08 V on the seventh cycle.

3.2.4. Effect of screen-printing number on utilization in batteries

Increasing the printing number in the preparation of the cathode on the substrate from 1 to 3, the weight of electroactive material ($Ni(OH)_2$) and the theoretical discharge capacity increases from 1.3 mg and 0.3757 mAh to 5.1 mg and 1.4739 mAh, respectively. The discharge capacity of batteries with various amounts of electroactive materials is found to be steady when the cycle number is

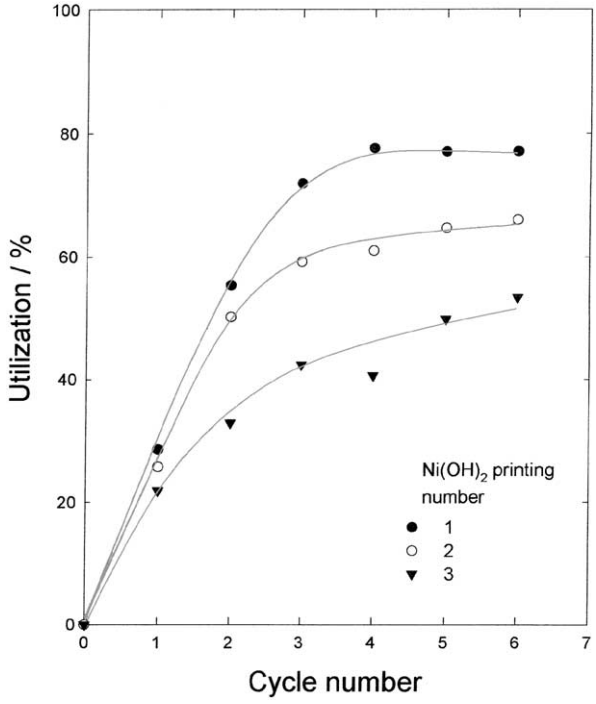

Fig. 13. Effect of charge–discharge cycle number on electroactive material utilization in batteries for various $Ni(OH)_2$ screen-printing numbers. Charge conditions: 0.10 C charged to 100% SoC. Discharge conditions: 0.02 C discharged to 0.95 V. Electrolyte: 5.347 M KOH and 0.477 M LiOH aqueous solution. Substrate: BP1100. Time for impregnation of electrolyte: 12 h.

greater than 5, as illustrated in Fig. 13. The increase in the steady discharge capacity from 0.2917 to 0.7875 mAh with increase in the screen-printing number from 1 to 3 is due to increase in the weight of $Ni(OH)_2$ from 1.3 to 5.1 mg. By contrast, the steady utilization in the battery decreases from 77.0 to 53.0% with increase in the printing number from 1 to 3 (Fig. 13). On increasing the printing number, the thickness of electroactive layer increases, as does the electric resistance between the electroactive materials and the current-collector. Therefore, utilization in the battery decreases with increase in the printing number.

4. Conclusions

The porosity of BP ceramic substrates decreases and the mechanical properties increase with increase in the annealing temperature in the final step. The fraction of the pore with a size between 10 and 300 μm on BP ceramic substrates increases with increase in the content (%) of ethyl cellulose in the BP argil. For example, on increasing the amount of ethyl cellulose in the argil from 0 to 0.79%, the mean pore diameter and the porosity increase from 0.0432 μm and 19.81% to 0.224 μm and 29.81%, respectively. The thickness of the alumina plate increases with increase in the weight of alumina powder and decrease in the pressure used for preparing the substrate. The effect of the time for impregnating electrolyte on the utilization in the battery is insignificant when the impregnation time is greater than 12 h at a reduced pressure of 0.03 atm. Using BP ceramic plates as substrates, the utilization in the battery increases from 68.8 to 74.9%, and the cycles required for obtaining steady utilization decreases from 7 to 5 with increase in the content of ethyl cellulose from 0 to 0.79%. When the pressure for preparing alumina substrates with 0.3 and 0.5 g Al_2O_3 powder is increased from 2.26×10^7 to 3.77×10^7 kg m^{-2}, the utilization in the battery decreases from 71.1 and 28.5% to 49.8 and 10.0%, respectively. The utilization in the battery increases from 53.0 to 77.0% when the weight of $Ni(OH)_2$ is decreased from 5.1 to 1.3 mg.

Acknowledgements

Financial support from the Ministry of Education of the Republic of China (Project number: EX-91-E-FA09-5-4) and Tunghai University is gratefully acknowledged.

References

[1] C.C. Liang, J. Electrochem. Soc. 16 (1969) 1322.
[2] J.B. Bates, N.J. Dudney, D.C. Lubben, G.R. Gruzalski, B.S. Kwak, X. Yu, R.A. Zuhr, J. Power Sources 54 (1995) 58.
[3] S.D. Jones, J.R. Akridge, J. Power Sources 54 (1995) 63.
[4] S.D. Jones, J.R. Akridge, Solid State Ionics 86–88 (1996) 1291.
[5] X. Yu, J.B. Bates, G.E. Jellison, F.X. Hart, J. Electrochem. Soc. 144 (1997) 524.
[6] P. Birke, W.F. Chu, W. Weppner, Solid State Ionics 93 (1997) 1.
[7] N.J. Dudney, B.J. Neudecker, Curr. Opin. Solid State Mater. Sci. 4 (1999) 479.
[8] B.J. Neudecker, R.A. Zuhr, J.B. Bates, J. Power Sources 81–82 (1999) 27.
[9] J.B. Bates, N.J. Dudney, B. Neudecker, A. Ueda, C.D. Evans, Solid State Ionics 135 (2000) 33.
[10] C. Branci, N. Benjelloun, J. Sarradin, M. Ribes, Solid State Ionics 135 (2000) 169.
[11] N.J. Dudney, J. Power Sources 89 (2000) 176.
[12] M. Nathan, E. Peled, D. Haronian, US Patent 6,197,450 (2001).
[13] W.C. West, J.F. Whitacre, V. White, B.V. Ratnakumar, J. Micromech. Microeng. 12 (2002) 58.
[14] P.H. Humble, J.N. Harb, R. LaFollette, J. Electrochem. Soc. 148 (2001) A1357.
[15] T. Sakai, I. Uehara, H. Ishikawa, J. Alloys Compounds 293–295 (1999) 762.